

LETTER

Nanoparticle generation from various types of silicon materials by nanosecond-pulsed laser irradiation

To cite this article: Ko Momoki and Jiwang Yan 2020 *Appl. Phys. Express* **13** 026505

View the [article online](#) for updates and enhancements.



Nanoparticle generation from various types of silicon materials by nanosecond-pulsed laser irradiation

Ko Momoki and Jiwang Yan*

Department of Mechanical Engineering, Faculty of Science and Technology, Keio University, Hiyoshi 3-14-1, Kohoku-ku, Yokohama, Kanagawa, Japan

*E-mail: yan@mech.keio.ac.jp

Received December 1, 2019; accepted January 8, 2020; published online January 29, 2020

A huge amount of silicon sludge is disposed of from silicon wafer manufacture, and its reuse is a critical issue. In this study, silicon nanoparticle generation from sludge was explored by nanosecond-pulsed laser irradiation. The nanoparticle production efficiency from silicon sludge was compared with that from silicon wafers. The result showed that using silicon sludge as a laser irradiation target leads to a distinctly higher production efficiency of nanoparticles; the smaller the powder size of the silicon sludge, the higher the efficiency. The generated silicon nanoparticles were crystalline with sizes at the 10 nm level. © 2020 The Japan Society of Applied Physics

Currently, in manufacturing processes of single- and poly-crystal silicon wafers, silicon ingots are sliced with a multi-wire saw, and subsequently the sliced wafers are finished by grinding and polishing to obtain mirror surfaces. However, during these abrasive machining processes, a large quantity of silicon sludge with a micrometer-level powder size is produced and disposed of as waste.¹⁾

On the other hand, silicon nanoparticles possess various unique and useful properties such as high photoluminescence, an intermediate band, a large surface area, and biocompatibility, some of which are distinctly different from those of bulk silicon.^{2–6)} These characteristics will improve the capabilities of lithium-ion batteries, solar cells, biomedical industries, and other high-value-added products.^{7–15)} One of the common methods to fabricate silicon nanoparticles is femtosecond-pulsed laser irradiation on a single-crystal silicon wafer.^{16–19)} However, it remains a very expensive and time-consuming process due to its low production efficiency.

In this study, we propose silicon nanoparticle generation by using a nanosecond-pulsed laser to irradiate silicon sludge. If the silicon sludge can be reused for silicon nanoparticle production, the energy and material resources can be saved effectively, and the industrial and economical advantage is huge. Moreover, a nanosecond-pulsed laser was adopted instead of a femtosecond-pulsed laser to examine the possibility of increasing nanoparticle generation efficiency. The fundamental nanoparticle generation behavior and production efficiency were investigated in comparison with those when using polished and ground silicon wafers as targets.

The silicon sludge used in the experiment had an average size of 3.9 μm , which was produced from a rough grinding process of silicon wafers. For the preparation of a target for laser irradiation, the silicon sludge was coated on a silicon wafer so that laser can be irradiated at a uniform distance from the silicon sludge. Before coating, the silicon sludge was mixed with an organic solvent of *N*-methyl-2-pyrrolidone and pulverized by a ball mill for 1, 2, and 3 h to obtain slurries with various powder sizes. The measurement result of the powder size distribution of the silicon sludge is shown in Fig. 1. The average powder size was 1.02, 0.83, and 0.60 μm (mode value: 0.72, 0.71, and 0.36 μm) after ball milling for 1, 2, and 3 h, respectively. Subsequently, the slurry was deposited on a silicon wafer to a thickness of 100 μm and dried at 100 °C for 2 h. For comparison, mirror-polished and ground single-crystal silicon (100) wafers were also used as targets.

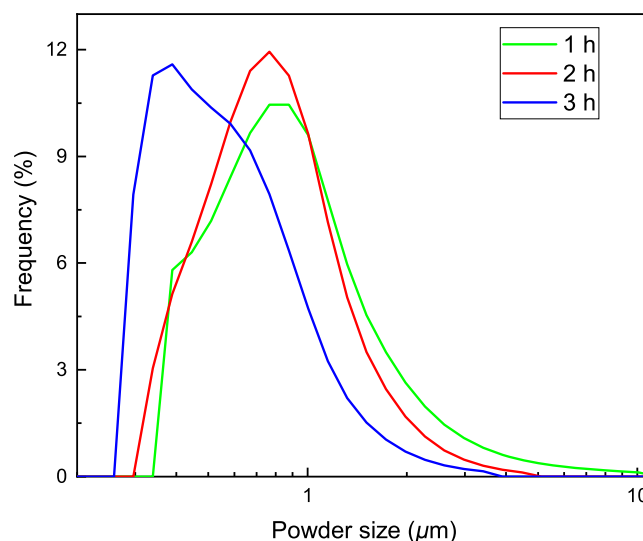


Fig. 1. (Color online) Powder size distribution of silicon sludge after ball milling for different lengths of time.

A nanosecond-pulsed Nd:YVO₄ laser system which had a wavelength of 532 nm, a frequency of 150 kHz, a pulse width of 38 ns and a spot diameter of 85 μm was used. The laser beam had a Gaussian energy distribution and was scanned using a galvanometer mirror system. The scan speed was set to 15 mm s⁻¹, and laser fluence was set to 1.0 and 2.0 J cm⁻².

Two methods were attempted to collect the generated silicon nanoparticles. One was to use a transparent glass substrate to cover the irradiated target in air where the distance between the target and the glass substrate was set to 100 μm . Upon laser irradiation through the glass, the silicon nanoparticles were backward-transferred and deposited on the glass substrate. The other was to use a membrane filter which had a pore size of 0.22 μm for nanoparticle collection in a vacuum chamber system. After laser was irradiated on the target, the generated silicon nanoparticles were pumped toward the filter and deposited on it.

After laser irradiation, the deposited silicon nanoparticles were observed using a scanning electron microscope (SEM; Inspect F50). Before SEM observation, a thin layer of osmium (thickness of ~5 nm) was coated on the samples. Moreover, the surface topography of the irradiated target was measured by a laser confocal microscope (OLS 4100), from which the amount of nanoparticle generation was calculated. Finally, the silicon nanoparticles were characterized by a transmission electron microscope (TEM; FEI Tecnai).

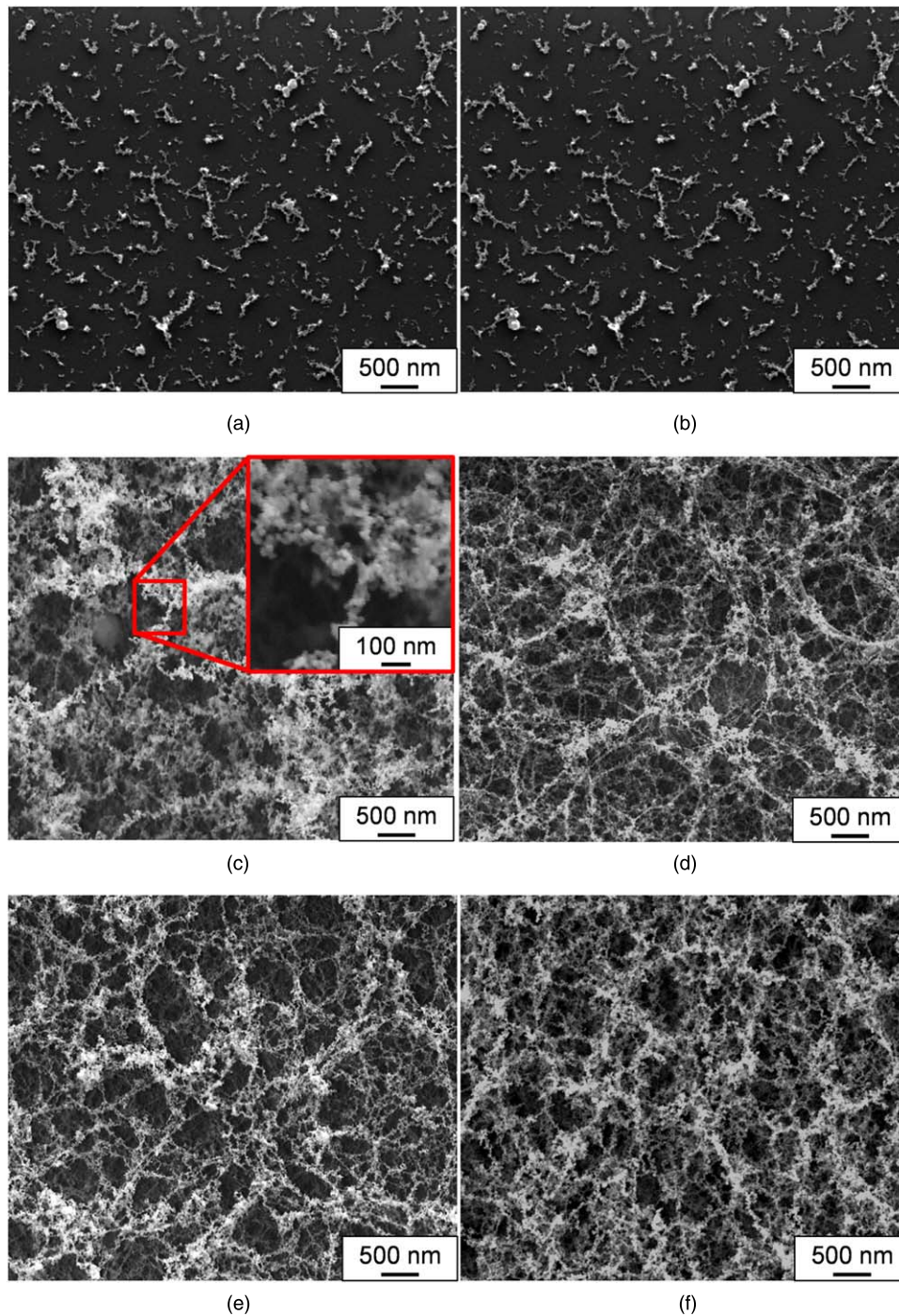


Fig. 2. (Color online) SEM images of silicon nanoparticles deposited on a glass substrate for various targets and laser fluences: (a) polished silicon wafer at 1.0 J cm^{-2} , (b) ground silicon wafer at 1.0 J cm^{-2} , (c) silicon sludge at 1.0 J cm^{-2} , (d) polished silicon wafer at 2.0 J cm^{-2} , (e) ground silicon wafer at 2.0 J cm^{-2} , (f) silicon sludge at 2.0 J cm^{-2} .

Figure 2 shows silicon nanoparticles deposited on the glass substrate. For all experimental conditions, nanoparticles (including coating) with a size of $\sim 20 \text{ nm}$ were successfully generated. For the silicon sludge, even at laser fluence of 1.0 J cm^{-2} , nanoparticle deposition was realized on the entire surface of the glass substrate [Fig. 2(c)]; when using a silicon wafer, however, silicon nanoparticles were hardly generated [Figs. 2(a) and 2(b)]. At 2.0 J cm^{-2} , all of the targets led to similar nanoparticle deposition morphology. However, the gaps among the nanoparticle networks were different. In the case of the silicon wafer targets, the gap size was greater

compared with that for silicon sludge, intuitively indicating that silicon sludge achieved a higher volume density of silicon nanoparticle deposition.

The deposition amount of nanoparticles per unit time, corresponding to the cross-sectional area multiplied by the scan speed, was obtained from cross-sectional profiles measured by the laser microscope, as shown in Fig. 3. At laser fluence of 1.0 J cm^{-2} , it is clear that the production efficiency of nanoparticles was greatly improved by using silicon sludge as a target. In the case of 2.0 J cm^{-2} , the production efficiency when using silicon sludge was still over

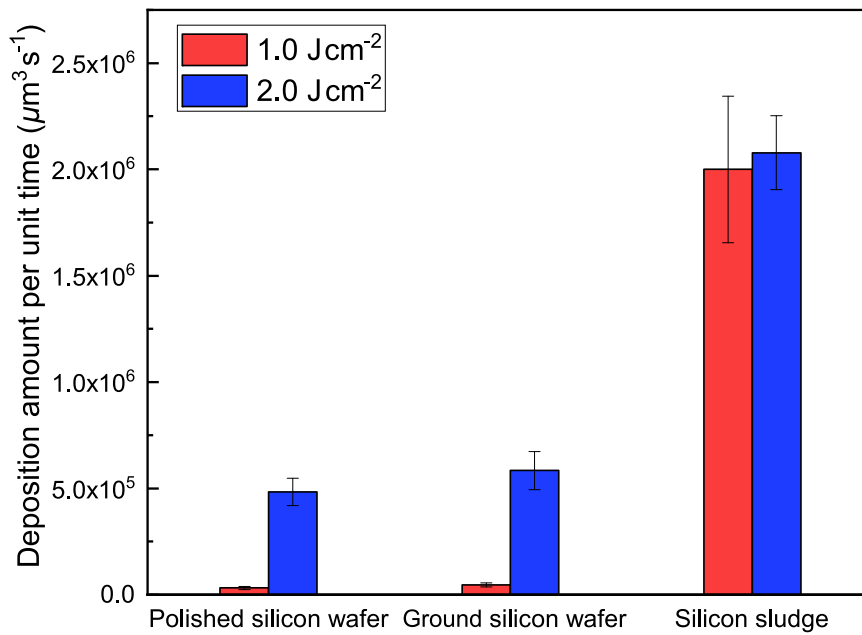


Fig. 3. (Color online) Deposition amount per unit time of various targets and laser fluences.

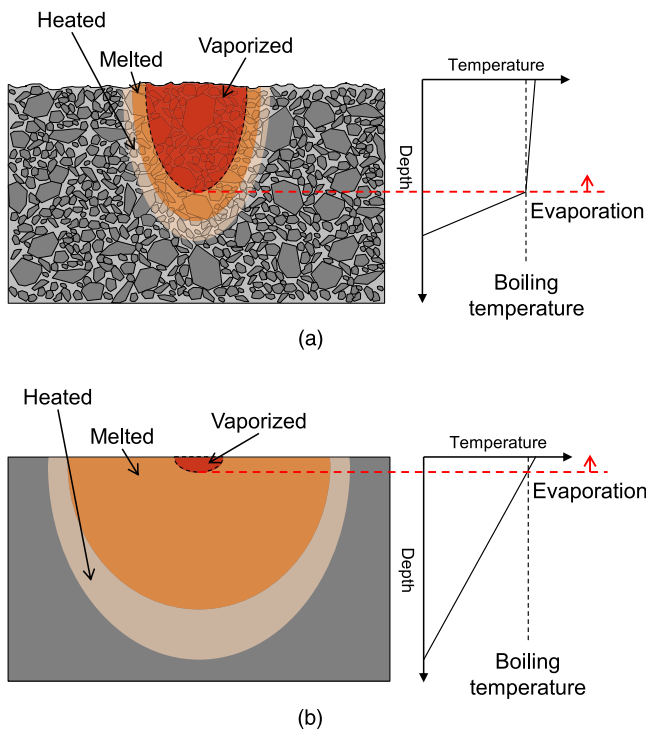


Fig. 4. (Color online) Schematic diagrams of the effect of thermal conductivity on material removal volume for different targets: (a) silicon sludge, (b) silicon wafers.

three times that when using silicon wafers, although the latter was also drastically increased. This result indicates that silicon sludge can achieve a higher production efficiency compared with silicon wafer even at lower laser fluence.

It is presumable that the difference in production efficiency was caused by the difference in thermal conductivity of the targets. It has been reported that the thermal conductivity for powder or a porous material decreases as compared with that for a bulk material.^{20–27} The effective thermal conductivity for silicon nanocrystals can be described using the following equation:²⁰

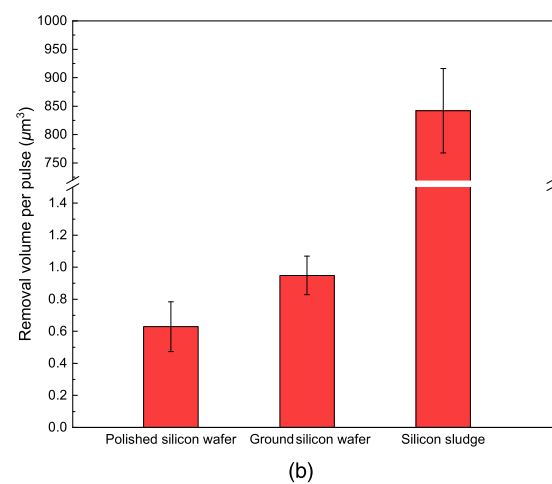
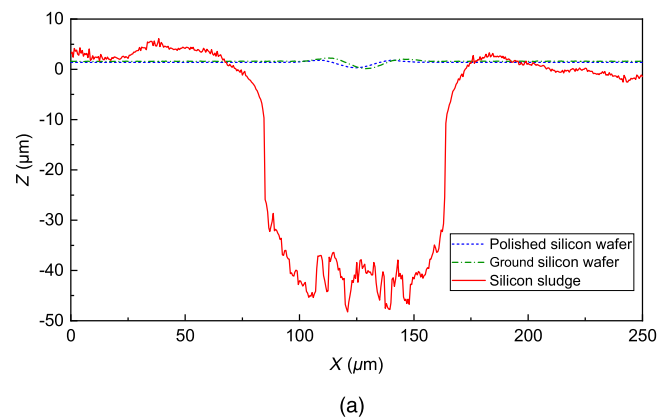


Fig. 5. (Color online) The material removal amounts for various irradiated targets at 2.0 J cm^{-2} : (a) cross-sectional profiles of targets, (b) material removal volume per pulse.

$$\kappa = \sum_p \frac{1}{3} \int C \cdot v \cdot \Lambda_{\text{eff}} \cdot d\omega, \quad (1)$$

where C is the spectral heat capacity, v the group velocity, ω the frequency and Λ_{eff} the effective mean free path. The

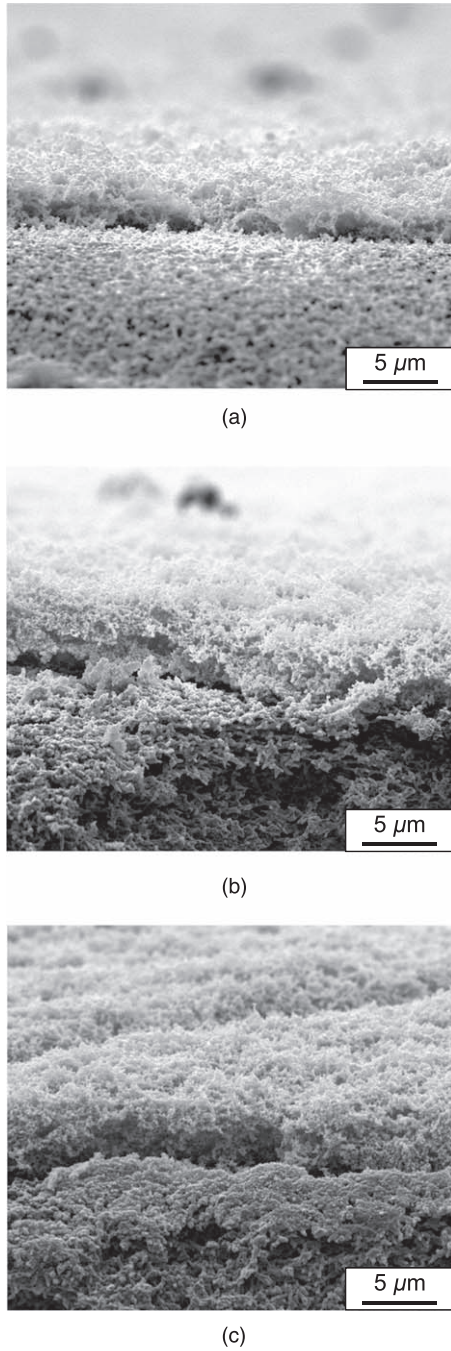


Fig. 6. Cross-sectional views of silicon nanoparticles generated from silicon sludge with various average powder sizes: (a) 1.02 μm , (b) 0.83 μm , (c) 0.60 μm .

phonon scattering including impurity/defect scattering Λ_{imp} , Umklapp scattering Λ_{umkl} , and grain boundary scattering Λ_{bdy} can be combined using Matthiessen's rule:

$$\Lambda_{\text{eff}}^{-1}(\omega, T) = \Lambda_{\text{imp}}^{-1}(\omega) + \Lambda_{\text{umkl}}^{-1}(\omega, T) + \Lambda_{\text{bdy}}^{-1}(\omega), \quad (2)$$

$$\Lambda_{\text{imp}}^{-1}(\omega) = \frac{A_1 \omega^4}{\nu}, \quad (3)$$

$$\Lambda_{\text{umkl}}^{-1}(\omega, T) = \frac{B_1 \omega^2 T \exp\left(-\frac{B_2}{T}\right)}{\nu}, \quad (4)$$

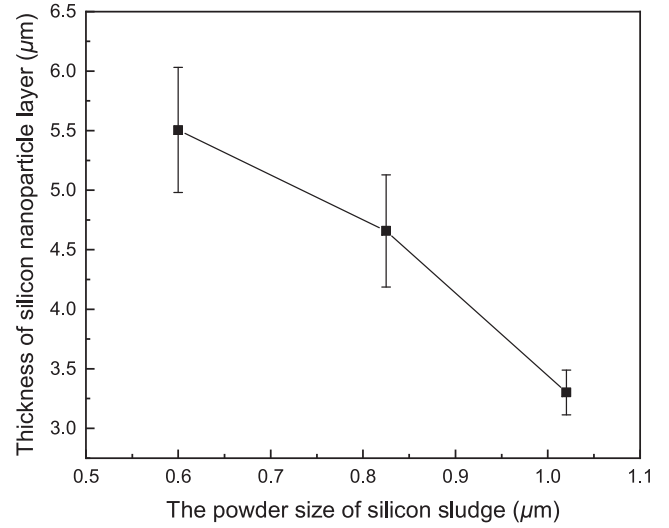


Fig. 7. Thickness change of silicon nanoparticle layer deposited on membrane filter.

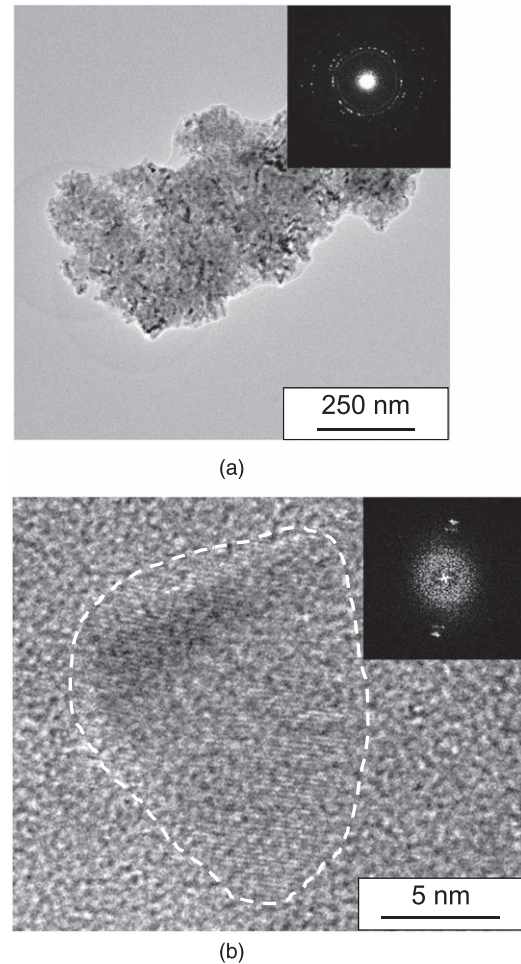


Fig. 8. TEM images and electron diffraction patterns of silicon nanoparticles: (a) aggregated nanoparticles, (b) a single nanoparticle.

$$\Lambda_{\text{bdy}}(\omega) = \alpha D_{\text{avg}} \left(\frac{\beta \omega_0}{\omega} \right), \quad (5)$$

where ω_0 is the maximum frequency, T the temperature, and D_{avg} the average powder size; A_1 , B_1 , B_2 , α , and β are parameters which can be determined by experimental fitting.

According to these equations, the effective thermal conductivity of a nano-sized powder material becomes far lower than that of a bulk material. Although the above equations cannot be quantitatively used for predicting the thermal conductivity of micro-sized powders due to the fact that the effective mean free path of phonons depends on the size of the powder, the effect of the grain boundary on phonon scattering should be similar qualitatively. For this reason, the effective thermal conductivity of silicon powder with a size of $\sim 1 \mu\text{m}$ is about $13 \text{ W m}^{-1} \text{ K}^{-1}$ which is distinctly lower than the thermal conductivity of bulk silicon ($70 \text{ W m}^{-1} \text{ K}^{-1}$ at a temperature of $\sim 500 \text{ K}$).^{20,23)} Thus, when laser was irradiated on the silicon sludge, the temperature distribution inside the silicon sludge might have been different from that of the silicon wafers, as presented in Fig. 4. If the input energy transferred by the laser is assumed to be the same, the integration of energy distribution must also be the same. In the case of the silicon sludge, the input energy might have been trapped due to its lower thermal conductivity [Fig. 4(a)], resulting in a drastic gradient of temperature distribution, whereas the temperature distribution inside the silicon wafers had a gentle gradient [Fig. 4(b)]. Therefore, the steeper temperature distribution in the silicon sludge contributed to a greater material removal amount in comparison with the silicon wafers.

The cross-sectional profiles of the targets were measured and the material removal volume per pulse was evaluated, as shown in Fig. 5. Apparently, the material removal amount of the silicon sludge sample was greater than those of both silicon wafers. In addition, the ground silicon wafer resulted in a 51% higher material removal amount than the polished silicon wafer. It is thought that the absorption coefficient caused the difference in material removal amount between the polished and ground silicon wafers. Laser intensity attenuation with laser penetration depth is given by the following equation:²⁸⁾

$$I(z) = (1 - R)I_0 \exp(-\alpha z) \quad (6)$$

where I is the laser intensity, z the laser penetration depth, R the reflection coefficient, I_0 the initial laser intensity, and α the absorption coefficient. After grinding, there remained machining-induced subsurface damage such as an amorphous layer. The absorption coefficient of amorphous silicon, α_a , is much higher than that of crystal silicon, α_c .^{29,30)} On the basis of Eq. (6), it can be predicted that different absorption coefficients lead to different material removal amounts.

Next, laser irradiation was carried out on silicon sludge with various powder sizes in a vacuum chamber system, and the obtained silicon nanoparticles were captured by a membrane filter. Cross-sectional views of the deposited nanoparticle layers are presented in Fig. 6. Moreover, the measured thickness of the silicon nanoparticle layer is plotted versus the powder size of the silicon sludge in Fig. 7. The result indicates that the layer of deposited silicon nanoparticles became thicker from 3.3 to $5.5 \mu\text{m}$ as the size of the silicon sludge decreased from 1.02 to $0.60 \mu\text{m}$. This might be due to the rise in total surface area of the silicon powder with its size reduction and the decrease in effective thermal conductivity. When volume is constant, a decrease in the size of the powder increases the total surface area, and in

turn, leads to higher surface reactivity since a relatively large fraction of component atoms are exposed on the surface.³¹⁾ Consequently, the surface energy rises. On the other hand, the effective thermal conductivity of silicon sludge strongly depends on its size according to Eq. (5). Therefore, nanoparticle production efficiency is improved by using smaller-sized silicon sludge.

Finally, TEM observation was performed on silicon nanoparticles generated from silicon sludge with a powder size of $1.02 \mu\text{m}$ at laser fluence of 1.0 J cm^{-2} , as presented in Fig. 8. The selected-area electron diffraction pattern of the agglomerated silicon nanoparticles in Fig. 8(a) shows that the aggregation had a polycrystalline phase. However, as seen from the magnified image of a single nanoparticle and its electron diffraction pattern in Fig. 8(b), the nanoparticle had a single-crystalline phase with a lattice plane of (220) corresponding to an interplanar spacing of $\sim 1.9 \text{ \AA}$. It is assumed that the integration of multiple diffraction patterns of individual silicon nanoparticles resulted in the polycrystalline-like phase.

In summary, nanosecond-pulsed laser irradiation was performed on silicon sludge and silicon nanoparticles were generated successfully. The nanoparticle production efficiency was compared with that when using polished/ground silicon wafers as targets. At the same laser fluence, a higher amount of silicon nanoparticles was obtained by using silicon sludge in comparison with silicon wafers due to the difference in effective thermal conductivity. The layer of deposited silicon nanoparticles became thicker as the powder size of silicon sludge decreased. The generated silicon nanoparticles were single crystals with an average size of $\sim 10 \text{ nm}$.

Acknowledgments This work has been partially supported by DISCO Corporation and the Japan Society for the Promotion of Science, under a Grant-in-Aid for Exploratory Research, 17K18833 (2017–2019).

ORCID iDs Jiwang Yan  <https://orcid.org/0000-0002-5155-3604>

- 1) A. Yoko and Y. Oshima, *J. Supercrit. Fluids* **75**, 1 (2013).
- 2) D. E. Harwell, J. C. Croney, W. Qin, J. T. Thornton, J. H. Day, E. K. Hajime, and D. M. Jameson, *Chem. Lett.* **32**, 1194 (2003).
- 3) Q. Wang, Y. Bao, X. Zhang, P. R. Coxon, U. A. Jayasooriya, and Y. Chao, *Adv. Healthc. Mater.* **1**, 189 (2012).
- 4) Z. Yuan, T. Nakamura, S. Adachi, and K. Matsuiishi, *Nanoscale* **9**, 1193 (2017).
- 5) T. G. Ulusoy Ghobadi, A. Ghobadi, T. Okyay, K. Topalli, and A. K. Okyay, *RSC Adv.* **6**, 112520 (2016).
- 6) S. Yang, W. Li, B. Cao, H. Zeng, and W. Cai, *J. Phys. Chem. C* **115**, 21056 (2011).
- 7) J. A. Carlisle, I. N. Germanenko, Y. B. Pithawalla, and M. S. El-Shall, *J. Electron Spectrosc. Relat. Phenom.* **114–116**, 229 (2001).
- 8) H. R. Rasouli, A. Ghobadi, T. G. Ulusoy Ghobadi, H. Ates, K. Topalli, and A. K. Okyay, *J. Opt.* **19**, 6 (2017).
- 9) X. Y. Chen, Y. Lu, Y. H. Wu, B. J. Cho, M. H. Liu, D. Y. Dai, and W. D. Song, *J. Anal. At. Spectrom.* **93**, 6311 (2003).
- 10) Y. Xin, T. Kitasako, M. Maeda, and K.-I. Saitow, *Chem. Phys. Lett.* **974**, 90 (2017).
- 11) L. Hu, H. Wu, S. Sae Hong, L. Cui, J. R. McDonough, S. Bohy, and Y. Cui, *Chem. Commun.* **47**, 367 (2011).
- 12) J. Sourice et al., *J. Power Sources* **328**, 527 (2016).
- 13) S. Goriparti, E. Miele, F. De Angelis, E. Di Fabrizio, R. Proietti Zaccaria, and C. Capiglia, *J. Power Sources* **257**, 421 (2014).
- 14) J. Lee, J. Koo, B. Jang, and S. Kim, *J. Power Sources* **329**, 79 (2016).
- 15) B. J. Dimitrijevic, K. E. Aifantis, and K. Hackl, *J. Power Sources* **206**, 343 (2012).
- 16) F. V. Kashav, T. P. Kaminskaya, and L. A. Golovan, *Opt. Quantum Electron.* **48**, 348 (2016).

- 17) E. I. Ageev, D. V. Potorochin, D. V. Sachenko, and G. V. Odintsova, *Opt. Quantum Electron.* **49**, 40 (2017).
- 18) U. Zywiets, C. Reinhardt, A. B. Evlyukhin, T. Birr, and B. N. Chichkov, *Appl. Phys. A* **114**, 45 (2014).
- 19) T. W. Reenaas, Y. S. Lee, F. R. Chowdhury, M. Gupta, Y. Y. Tsui, T. Y. Tou, S. L. Yap, S. Y. Kok, and S. S. Yap, *Appl. Surf. Sci.* **354**, 206 (2015).
- 20) T. Suzuki, Y. Ohishi, K. Kurosaki, H. Muta, and S. Yamanaka, *Appl. Phys. Express* **5**, 081302 (2012).
- 21) Z. Wang, J. E. Alaniz, W. Jang, J. E. Garay, and C. Dames, *Nano Lett.* **11**, 2206 (2011).
- 22) A. Wolf and R. Brendel, *Thin Solid Films* **513**, 385 (2006).
- 23) S. P. Ashby, T. Bian, H. Ning, M. J. Reece, and Y. Chao, *J. Electron. Mater.* **44**, 1931 (2015).
- 24) J. H. Seol, D. S. Barth, J. Zhu, D. C. Coso, K. Hippalgaonkar, J. Lim, J. Han, X. Zhang, and A. Majumdar, *Appl. Phys. Lett.* **111**, 1 (2017).
- 25) Q. Shen and T. Toyoda, *Rev. Sci. Instrum.* **74**, 601 (2003).
- 26) Y. Liu, S. Zhang, Z. Han, and Y. Zhao, *J. Nanoparticle Res.* **18**, 1 (2016).
- 27) B. K. Jang and Y. Sakka, *J. Alloys Compd.* **463**, 493 (2008).
- 28) J. Yan and F. Kobayashi, *CIRP Ann. - Manuf. Technol.* **62**, 199 (2013).
- 29) K. Juraić, D. Gracin, I. Djerdj, A. Lausi, M. Čeh, and D. Balzar, *Nucl. Instrum. Methods Phys. Res., Sect. B* **284**, 78 (2012).
- 30) V. Jovanov, J. Ivanchev, and D. Knipp, *Opt. Express* **18**, 426 (2010).
- 31) H. Krupp, *Adv. Colloid Interface Sci.* **1**, 111 (1967).